Kane's[16] theory we have calculated the variation of the effective mass of an electron with the magnetic field due to the nonparabolicity of the band. In the case of CdTe, for instance, we find that this variation from the zero field mass is about 1.5% at 100 kG. The corresponding variation in the polaron mass is about 4%. For GaAs, however, the change in the effective mass due to the nonparabolicity of the band is about 2% at 100 kG whereas the variation in the polaron mass is about 0.4%. It seems that, in most direct wide-energy-gap ionic semiconductors, the effects due to the nonparabolicity of the conduction band are relatively small.

Cyclotron-resonance experiments in several III-V compounds have been made[17] and a small change in the effective mass of an electron as a function of the magnetic field is observed. In GaAs for instance, we find that the observed variation of the cyclotron mass with field is the same as we have calculated. Similar measurements in II-VI compounds have not yet been made.

## ACKNOWLEDGMENTS

The author wishes to thank Professor Sergio Rodriguez for many useful discussions. He would also like to thank his wife, Mrs. Swarn Bajaj, for clarifying some mathematical points.

[16] E. O. Kane, J. Phys. Chem. Solids 1, 249 (1957).

[17] E. D. Palik, S. Teitler, and R. F. Wallis, J. Appl. Phys. Suppl. 32, 2132 (1961). See also references to previous work mentioned in this article.

PHYSICAL REVIEW VOLUME 170, NUMBER 3 15 JUNE 1968

# Raman Scattering in 6*H* SiC†

D. W. Feldman, James H. Parker, Jr., W. J. Choyke, and Lyle Patrick
*Westinghouse Research Laboratories, Pittsburgh, Pennsylvania 15235*

(Received 27 December 1967)

Fifteen phonon lines were observed in the first-order Raman spectrum of 6*H* SiC, using laser excitation. Polarized light was used to identify the mode symmetry, and a large-zone analysis was used to classify the modes and to display the results in what appear to be dispersion curves. All observed narrow lines are consistent with our interpretation, and only two of the expected lines remain unobserved. A study of the dependence of phonon energy on propagation direction shows that certain infrared and Raman active modes have extremely little infrared strength (a consequence of the polytype structure of 6*H* SiC). Doublets in the Raman spectrum give accurate measurements of the 4–8-cm$^{-1}$ discontinuities within the large zone.

## I. INTRODUCTION

RAMAN measurements have been greatly improved by the use of laser light sources. In recent Raman work the allowed optical phonons of ZnO [1] and CdS [2] have been fully identified. These crystals are uniaxial, with wurtzite structure. 6*H* SiC belongs to the same space group as ZnO and CdS ($P6_3mc$) but has more atoms per unit cell,[3] and therefore has additional weak modes accessible to Raman scattering. As a result of certain special properties of phonons in SiC polytypes it is possible to classify the observed weak modes in 6*H* SiC and to display the results in what appear to be phonon dispersion curves.

Many phonon energies have been reported for 6*H* SiC, but most are zone boundary phonons, measured in luminescence,[4] indirect interband absorption,[5] and two-phonon infrared absorption.[6] Polytype 6*H* has 12 atoms per unit cell, hence 33 long-wavelength optic modes, many of them allowed in first-order Raman scattering, but few of them previously observed. Earlier Raman work on SiC was done without a laser, and apparently without polytype identification; only a few lines were reported.[7] The residual ray reflection spectrum of 6*H* SiC was analyzed by Spitzer *et al.*[8] to give fairly complete information on the strong modes. Recently[9] an additional weak absorption line was found at 19.9 $\mu$. This was subsequently identified as a fundamental lattice line, the key to identification being an analysis of phonon branches in the large zone.[10]

† This work was supported in part by the U. S. Air Force Materials Laboratory, Wright-Patterson Air Force Base, Ohio, under Contract No. F33615-67-C1401.

[1] T. C. Damen, S. P. S. Porto, and B. Tell, Phys. Rev. 142, 570 (1966).

[2] B. Tell, T. C. Damen, and S. P. S. Porto, Phys. Rev. 144, 771 (1966).

[3] A. R. Verma and P. Krishna, *Polymorphism and Polytypism in Crystals* (John Wiley & Sons, Inc., New York, 1966).

[4] W. J. Choyke and Lyle Patrick, Phys. Rev. 127, 1868 (1962). Table I lists 17 phonon energies, but only one component of the wave vector was identified. The energy conversion factor is 1 meV = 8.07 cm$^{-1}$.

[5] Reference 4, Sec. VII.

[6] Lyle Patrick and W. J. Choyke, Phys. Rev. 123, 813 (1961).

[7] J. P. Mathieu and H. Poulet, Compt. Rend. 244, 2794 (1957).

[8] W. G. Spitzer, D. A. Kleinman, and D. Walsh, Phys. Rev. 113, 127 (1959).

[9] B. Ellis and T. S. Moss, Proc. Roy. Soc. (London) 299, 393 (1967).

[10] Lyle Patrick, Phys. Rev. 167, 809 (1968).

Two large SiC crystals were cut and polished for the present Raman experiment. They were examined for polytype in Laue transmission photographs and found to be pure 6H. With the use of an argon ion laser for excitation, both strong and weak one-phonon Raman lines were observed, the same fifteen lines in both crystals. The mode symmetry was identified by the use of polarized light (both incident and scattered).[11] The identification of phonon branch and position in the large zone then followed with minimal reliance on plausibility arguments.

## II. PHONONS IN SiC POLYTYPES

A systematic study of phonons in SiC polytypes is made easier by the use of a standard large zone for all polytypes, as explained in Ref. 10. The large zone for polytype 6H is reviewed here briefly, and the distinction between strong and weak modes is emphasized. The high anisotropy of the weak modes leads to a classification of modes with respect to the two limiting conditions considered by Loudon for uniaxial crystals.[11] The two groups identified in this way are identical with the strong and weak groups, identified by their positions in the large zone.

### A. Standard Large Zone

For long-wavelength phonons we need to consider only the axial direction of the large zone.[12] The standard large zone for 6H SiC extends to $6\pi/c$, where $c$ is the axial dimension of the unit cell. Since $2\pi/c$ is a reciprocal lattice vector, the pseudomomentum vectors $q=0$, $2\pi/c$, $4\pi/c$, and $6\pi/c$ are all equivalent to $q=0$ in the Brillouin zone. Thus, if we define a reduced momentum $x=q/q_{\max}$, the values of $x$ accessible to Raman scattering measurements are $x=0$, 0.33, 0.67, and 1; vertical lines are erected at these points in Fig. 1. The phonon branches in the large zone are labeled as follows, from top to bottom in Fig. 1(a): axial optic (single), planar optic (double), axial acoustic (single), and planar acoustic (double). The dispersion curves, when drawn this way, are expected to be nearly independent of polytype[13]; it is the values of $x$ corresponding to long-wavelength modes that depend on the polytype (these are listed for several polytypes in Table I of Ref. 10).

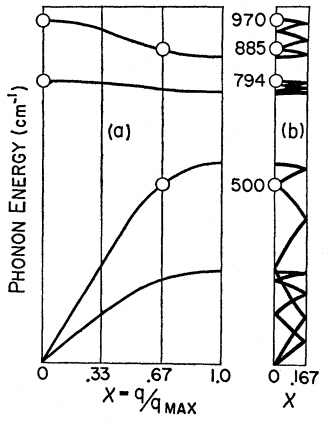


FIG. 1. The axial direction dispersion curves (largely schematic) for phonons in 6H SiC: (a) in the large zone, and (b) folded into the Brillouin zone. Open circles indicate the four optical modes measured in infrared reflection or absorption (see Ref. 10). The abscissa is $x=q/q_{\max}$, where $q_{\max}=6\pi/c$. For all optical modes, $q=0$ in the Brillouin zone; in the large zone the strong optical modes appear at $x=0$, and the weak optical modes at $x=0.33$, 0.67, or 1.

TABLE I. Distribution and symmetry type of phonon modes in the large zone. The modes at $x=0$ are strong or truly acoustic (ac.); all modes at $x\neq 0$ are weak. There are double sets of representations at $x=0.33$ and 0.67, where internal energy discontinuities occur. It is assumed that there is no longitudinal, transverse splitting of $E_1$ modes. Thus, the assignment of representations for the strong modes are valid only for the propagation direction $\theta=0°$. The modes total $6(A_1+B_1+E_1+E_2)$.

| Branch | $x=0$ | $x=0.33$ | $x=0.67$ | $x=1$ |
|---|---|---|---|---|
| Axial optic | $A_1$ (strong) | $2B_1$ | $2A_1$ | $B_1$ |
| Planar optic | $E_1$ (strong) | $2E_2$ | $2E_1$ | $E_2$ |
| Axial acoustic | $A_1$ (ac.) | $2B_1$ | $2A_1$ | $B_1$ |
| Planar acoustic | $E_1$ (ac.) | $2E_2$ | $2E_1$ | $E_2$ |

The phonon branches shown in Fig. 1 are partly known, partly schematic. They are based on (a) the four points determined by infrared measurements, shown by open circles, (b) knowledge of phonon energies elsewhere in the zone, and (c) analogy with the known Ge and Si phonon dispersion curves in the [111] direction. In assigning observed Raman lines to the intersections of the dispersion curves with the vertical lines, one also uses the fact that the phonon representation ($A_1$, $E_1$, or $E_2$) is experimentally determined by the use of polarized light.[11] It was shown in Ref. 10 that $A_1$ and $E_1$ modes should be assigned to $x=0$ or 0.67, and $E_2$ modes to $x=0.33$ or 1. The distribution of phonon modes by symmetry type is shown in Table I. The $B_1$ modes are not observable, either in infrared or in Raman measurements.[14] Note that there are double sets of representations at $x=0.33$ and 0.67 because of the energy discontinuities at these internal boundaries.

The large-zone concept is most useful when the energy discontinuities are small. For 6H SiC the doublet structure in the present Raman data provides the first accurate measurement of these discontinuities.

### B. Strong and Weak Modes

In most physical properties SiC polytypes have obvious similarities but subtle differences. For example, the

[11] R. Loudon, Advan. Phys. 13, 423 (1964).

[12] SiC polytype structures are characterized by a one-dimensional stacking sequence of planes. Consequently, the large zone is extended in only one direction, the axial direction, and all long-wavelength modes are found on the large-zone axis.

[13] The concept of a common spectrum for all polytypes was introduced as a hypothesis in Ref. 10 and will be checked by Raman measurements on other SiC polytypes.

[14] $A_1$ and $B_1$ are axial modes ($\|$ in Ref. 11); the doubly degenerate $E_1$ and $E_2$ modes are planar ($\perp$ in Ref. 11).

strong residual ray absorption ($>10^5$ cm$^{-1}$) appears to be nearly independent of polytype in frequency and intensity,[15] but most polytypes have additional weak infrared absorption lines ($\approx 10^2$ cm$^{-1}$) that are characteristic of the polytype.[9] The separation of infrared modes into strong and weak is clear and unambiguous from the large-zone point of view[10]; phonons at the large-zone center are strong and independent of polytype, whereas all others are weak (or forbidden) and have values of $x$ that are characteristic of the polytype.

The separation into strong and weak modes is also appropriate for Raman scattering, although the differences in line intensities ($\approx 10^2$) are not as striking as those in the infrared ($\approx 10^3$), and there is a great variation in strength within the group of weak lines. It is convenient to retain the terminology "strong" and "weak" for modes at $x=0$ and at $x\neq 0$, respectively, even though Raman intensity is not the only criterion for the division into two groups.

From the large-zone point of view the weak modes, with $x\neq 0$, appear to have a short wavelength; from the Brillouin-zone point of view this motion is intracell, with equivalent atoms in all unit cells vibrating in phase. The absence or presence of intracell motion also distinguishes strong and weak modes, and it is this motion that is responsible for the high anisotropy of the weak modes.

### C. Anisotropy

Optical modes in polar uniaxial crystals may be classified according to the dominance of (a) the long-range electrostatic field, or (b) crystal anisotropy.[11] The form of the dependence of phonon frequency on propagation and polarization directions simplifies for the limiting cases discussed by Loudon, (a)$\gg$(b) or (b)$\gg$(a). The 6$H$ SiC optical modes all satisfy one or the other of these two limiting conditions.[10] For the strong $x=0$ modes (a)$\gg$(b), whereas for the weak $x\neq 0$ modes (b)$\gg$(a). Thus, the optical modes are grouped in the same way whether classified by the large-zone method or by the Loudon limits.

The two groups of optical modes have quite different behavior for propagation in a general direction $\theta\neq 0°$ or 90°, where $\theta$ is the angle between the propagation vector and the $c$ axis.[16] The angular dependence is illustrated in Fig. 2. The strong modes are primarily longitudinal or transverse because of the long-range electric field, but they have mixed symmetry type ($A_1+E_1$). There is a large separation in frequency of longitudinal and transverse modes, due to the field, and a small dependence of either frequency on the angle $\theta$, due to the low but measurable anisotropy of the strong modes at $x=0$.

On the other hand, the weak modes with (b)$\gg$(a) are primarily axial or planar, i.e., the vibrational motion is largely along or perpendicular to the $c$ axis, with a large separation in frequency because of the high anisotropy of the weak modes. In a general propagation direction these modes retain their symmetry type, but the weak infrared-allowed $A_1$ and $E_1$ modes have a mixed longitudinal and transverse character which depends on $\theta$ and which could, in principle, lead to an angular dependence of the frequency. However, the one weak $A_1$ mode observed in infrared absorption[9] is so weak (absorption constant about 100 cm$^{-1}$) that the expected total angular energy dependence as this mode changes from longitudinal at $\theta=0°$ to transverse at $\theta=90°$ would be less than a wave number, too small to measure.

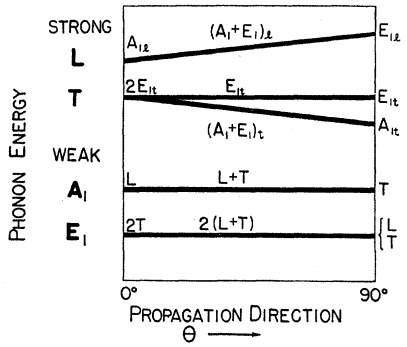


FIG. 2. Schematic comparison of the angular dependence of strong $A_1$ and $E_1$ modes with that of weak $A_1$ and $E_1$ modes. When the propagation vector $q$ lies in a symmetry direction, $\theta=0°$ or 90°, both strong and weak modes can be characterized as longitudinal (L) or transverse (T), and also as axial ($A_1$) or planar ($E_1$). In a general direction, $\theta\neq 0°$ or 90°, strong modes remain L or T, but have mixed $A_1$ and $E_1$ character; weak modes remain $A_1$ or $E_1$ but have mixed L and T character. The angular dependence of energy of two of the strong modes is due to crystal anisotropy. The angular dependence of energy of the weak modes is due to the long-range electric field, and is expected to be negligible.

## III. EXPERIMENTAL

### A. Equipment and Procedures

The Raman spectra were excited with 4880 Å light from an argon ion laser with a power output of about 400 mW. Because of Brewster windows on the laser discharge tube, the exciting light was highly polarized in a vertical plane. The Raman light was observed in a direction at right angles to the direction of the exciting light. By a suitable arrangement of prisms the scattered light could be observed in a direction either parallel to or normal to the polarization direction of the incident light. After passing through a polarizer, the Raman radiation was dispersed by a double tandem monochromator (Spex 1400) and detected with a cooled S-11 photomultiplier. Because of the finite acceptance angle of the monochromator ($f$ 6.8), the scattered light observed was as much as 5° away from the nominal direction.

The wavelengths of the Raman lines were measured with respect to known lines from a low-pressure neon

[15] W. G. Spitzer, D. A. Kleinman, and C. J. Frosch, Phys. Rev. 113, 133 (1959).

[16] The atomic motion is determined by the propagation vector for strong modes, by the crystal axis for weak modes.

lamp. The uncertainties in the Raman frequencies are less than 2 $cm^{-1}$.

Two 6*H* SiC crystals, from different furnace runs, were cut into rectangular parallelepipeds and polished. They measured 3×9×0.9 mm and 3×6×0.8 mm, with the small dimension in the direction of the *c* axis. They were relatively pure chemically, as judged by transparency, and pure polytypes, as judged by transmission Laue photographs. The crystals were at room temperature for all measurements.

### B. Notation and Selection Rules

Because 6*H* SiC has the same symmetry as the wurtzite structure, $C_{6v}$, we can refer to previous work for (1) normal-mode symmetry, (2) components of the tensors of change in polarizability on excitation of a normal mode, and (3) vector diagrams illustrating scattering and polarization relationships. A convenient source is Ref. 1, and we therefore use the four-letter notation of Damen *et al.* for the propagation and polarization symbol.

Reference axes *x*, *y*, and *z* are fixed in the crystal, with *z* along the *c* axis. A four-letter symbol, for example, $x(zx)y$, consists of a propagation part $x(--)y$ and a polarization part $-(zx)-$; the part $x(--)y$ means that light incident along the *x* axis is scattered along the *y* axis, and the part $-(zx)-$ means that the polarization directions of incident and scattered light are *z* and *x*, respectively. In this example the scattering plane is *xy*, and conservation laws determine the phonon propagation direction in the plane. The photon polarization directions, $-(zx)-$, determine one component of a tensor. The polarization-change tensors given in Ref. 1 show that, for this component, the Raman scattered mode would have $E_1$ symmetry.

In Table II we simply list the allowed normal-mode symmetry or symmetries for each tensor component. We also list the phonon propagation directions for the crystal orientations used in this experiment. For $C_{6v}$ symmetry this direction is sufficiently defined by giving the angle $\theta$ that it makes with the *c* axis.

The number of possible Raman lines is greater for 6*H* SiC than for wurtzite because the normal modes are

TABLE II. Significance of polarization and propagation symbols for the identification of phonon symmetry and propagation direction. The polarization symbols are the six components of a symmetric tensor. For $C_{6v}$ symmetry the corresponding allowed phonon representations are listed (see Refs. 1 or 11 for details). The propagation symbols indicate the two phonon propagation directions used in the present experiment.

| Polarization symbol | Phonon symmetry | Propagation symbol | Propagation angle $\theta$ |
|---|---|---|---|
| $-(xx)-$ | $A_1, E_2$ | $x(--)y$ | 90° |
| $-(yy)-$ | $A_1, E_2$ | $z(--)x$ | 45° |
| $-(zz)-$ | $A_1$ | | |
| $-(xy)-$ | $E_2$ | | |
| $-(yz)-$ | $E_1$ | | |
| $-(zx)-$ | $E_1$ | | |

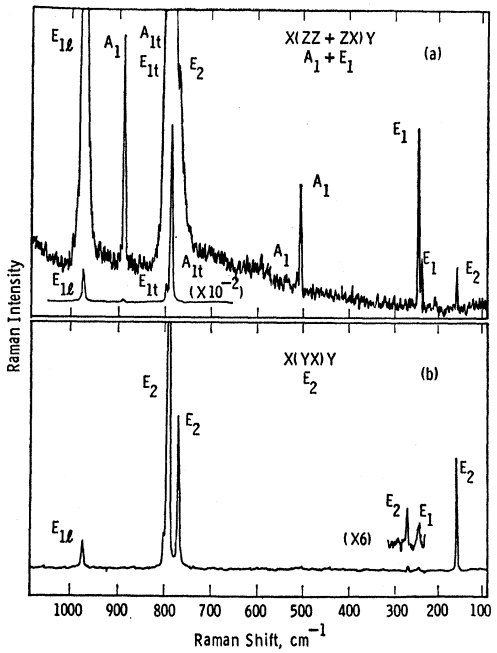


FIG. 3. Raman spectrum, showing full range of the one-phonon-emission part, with arrangements permitting (a) $A_1$ and $E_1$ modes, and (b) $E_2$ modes. The broad background in (a) is probably second order, which is strong in $A_1$ combinations.

$6(A_1+B_1+E_1+E_2)$ instead of $2(A_1+B_1+E_1+E_2)$. However, the only new problem is distinguishing between several normal modes of the same symmetry, and that is the reason for introducing the large zone.

### C. Results

The first-order Raman spectrum[17] is shown in four figures, of which the first shows the entire energy range, and the other three show details not observed in the first. The polarization arrangement of Fig. 3(a) was chosen to show a large number of lines. The symbol $x(zz+zx)y$ indicates that only the incident light was polarized (*z*) and that the scattering plane was *xy*, i.e., $\theta=90°$. Table II shows that the polarization components $-(zz)-$ and $-(zx)-$ permit the observation of $A_1$ and $E_1$ modes, respectively. Two unallowed $E_2$ modes appear weakly because of the finite acceptance angle of the monochromator. An inset shows the strong modes $E_{1l}$, $E_{1t}$, and $A_{1t}$ with intensity reduced by a factor of 100. The arrangement of Fig. 3(b) retains the *xy* scattering plane, and the polarization $-(yx)-$ permits observation of $E_2$ modes. Two unallowed $E_1$ modes appear weakly. There seem to be three moderately intense and one very weak $E_2$ lines, but Fig. 4 shows an $E_2$ doublet at 145 and 149 $cm^{-1}$ with the first component extremely weak. Thus, a total of five $E_2$ lines are observed of the possible six. All the weak lines were reproducible and were found in both samples.

[17] The lines assumed to be first order have a half-width of 4 $cm^{-1}$ or less. All other lines are much wider.

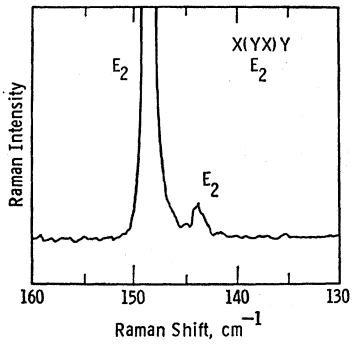


FIG. 4. Portion of Raman spectrum, with scale expanded to show an $E_2$ doublet.

Insertion of a polarizer in the scattered beam made it possible to separate the $A_1$ and $E_1$ spectra, and thus to identify the symmetry type of the lines shown in Fig. 3(a). An example of a portion of the spectrum with polarizer inserted is shown in Fig. 5. The very intense $A_{1t}$ is easily separated, but can also be seen in the $x(zx)y$ arrangement, which should allow only $E_1$. However, a comparison of intensities here and in Fig. 3(a) leaves no doubt that these lines are correctly identified. Remnants of unallowed lines cannot be avoided with the 5° acceptance angle of the monochromator, but relative intensities under different arrangements are used to complete the identification of the mode symmetry.

In correlating the various figures it is helpful to use a schematic drawing (Fig. 6) showing all first-order lines, including some not yet shown in the data. Four degrees of relative intensity are indicated, based on the strongest appearance of each line in the various arrangements used. The "strong" modes, previously identified in infrared reflection measurements, are the three most intense, as expected; their symmetry symbols have a second subscript to indicate longitudinal ($l$) or transverse ($t$). Both the notation and the energies of the strong modes depend on the propagation direction. Those shown in Fig. 6 are appropriate for $\theta=90°$. Two lines are coincident at 788 cm$^{-1}$, the very intense $A_{1t}$ and one of the $E_2$ lines. These are separately identified by the use of polarized light in Figs. 3(a) and 3(b), but can also be separated in energy by changing the crystal orientation so as to change the phonon propagation direction, as indicated below.

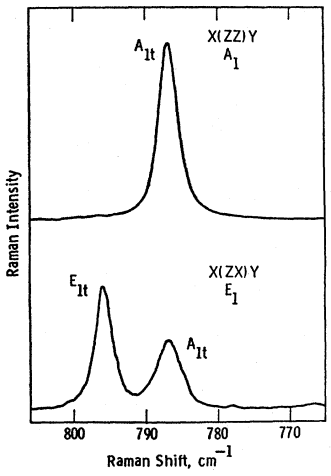


FIG. 5. Portion of Raman spectrum, showing the separation of $A_1$ and $E_1$ components by means of a polarizer. Intensity comparisons with Fig. 3(a) are used to confirm the identification.

To study the angular dependence of phonon energies, the crystal was oriented so as to make the scattering plane $xz$ (or $yz$). This changes the phonon propagation angle to $\theta=45°$. The weak mode part of the Raman spectrum is not shown for $\theta=45°$ because the line positions are the same as in the $\theta=90°$ spectrum, within the experimental limits (2 cm$^{-1}$). No change was expected for the infrared *inactive* $E_2$ modes, but it is significant that the weak infrared *active* $A_1$ and $E_1$ modes also were unchanged. Any change would give a measure of their infrared strength, since the weak mode angular variation of energy is determined by the long-range Coulomb field. Thus, our results show the extreme weakness of the additional infrared active modes that owe their existence to the polytype structure of 6$H$ SiC.

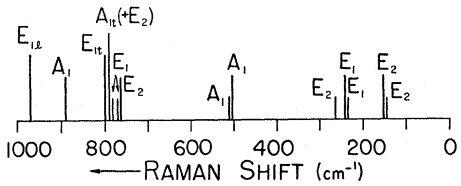


FIG. 6. Schematic showing all 15 lines, with a rough classification into four degrees of relative intensity. Two lines are coincident at 788 cm$^{-1}$ ($A_{1t}$ and $E_2$).

The angular energy dependence of the strong modes due to crystal anisotropy was found to be small but measurable. One of the three modes remains $E_{1t}$ and stays at 797 cm$^{-1}$. $E_{1l}$ at $\theta=90°$ changes to $(E_1+A_1)_l$ at 45°, and moves from 970 to 967 cm$^{-1}$. $A_{1t}$ at $\theta=90°$ changes to $(A_1+E_1)_t$ at 45° and moves from 788 to 792 cm$^{-1}$. This line and the other five in the planar optic branch are shown in Fig. 7(a). The symbol $x(zx+zy)z$ indicates that only the incident light is polarized. The polarization components $-(xz)-$ and $-(zy)-$ both allow only $E_1$ modes; a mixed mode like $(A_1+E_1)_t$ is excited through the $E_1$ portion. The two $E_2$ modes allowed by the arrangement of Fig. 7(b) also come through weakly in Fig. 7(a), enabling us to see six closely spaced planar optic lines. The $E_2$ line at 788 cm$^{-1}$ is unchanged at $\theta=45°$, but the $(A_1+E_1)_t$ line shifts enough to resolve the $\theta=90°$ coincidence. An extremely weak $E_1$ pair at 769 and 777 cm$^{-1}$ are shown in the inset.

## IV. DISCUSSION OF RESULTS

The experimental results will be discussed in three parts: (a) the strong modes and their angular depen-

dence, (b) weak modes and their assignments to values of $x=q/q_{max}$ in the large zone, and (c) doublet structure in the Raman spectrum as a measure of energy discontinuities in the large zone.

### A. Strong Modes

The three strong modes were observed with two crystal orientations such that the propagation angles were $\theta=90°$ and 45°, and the measured energies are listed in Table III. Two of the modes have an angular variation of energy given by

$$\omega_T^2(\theta)=(788)^2\sin^2\theta+(797)^2\cos^2\theta \quad (1)$$

and

$$\omega_L^2(\theta)=(A_{1l})^2\cos^2\theta+(970)^2\sin^2\theta, \quad (2)$$

where we have put our experimental values into Loudon's formulas.[18] Our measured value of $(A_1+E_1)_t$ at $\theta=45°$ is consistent with Eq. (1). We use Eq. (2) and our measured value of $(A_1+E_1)_l$ at $\theta=45°$ to obtain $A_{1l}=964$ cm$^{-1}$. Thus we obtain the phonon energies at $\theta=0°$ without a measurement[19]; they are shown in parentheses in Table III.

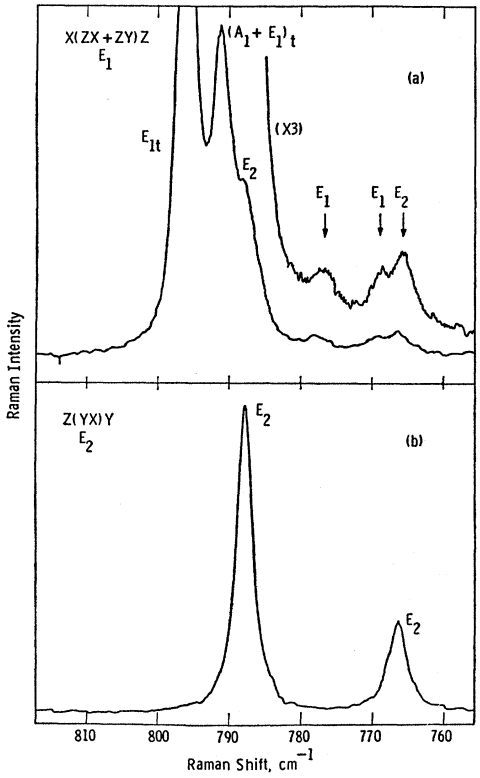


FIG. 7. Portion of Raman spectrum showing six lines of the planar optic branch, with experimental arrangements permitting (a) $E_1$ modes, and (b) $E_2$ modes.

[18] Reference 11, p. 430.

[19] For such a measurement, with phonon propagation along the $c$ axis, a special crystal cut would be required; see Ref. 1.

TABLE III. Dependence on propagation angle $\theta$ of the energy of the strong modes (in cm$^{-1}$). One mode is longitudinal (L), and two are transverse ($T_1$ and $T_2$). The figures in parentheses for $\theta=0°$ are derived, not experimental. $E_{1t}$ is doubly degenerate at $\theta=0°$.

| | $\theta=90°$ | $\theta=45°$ | $\theta=0°$ |
|---|---|---|---|
| L | $E_{1l}$ 970 | $(A_1+E_1)_l$ 967 | $A_{1l}$ (964) |
| $T_1$ | $E_{1t}$ 797 | $E_{1t}$ 797 | $E_{1t}$ (797) |
| $T_2$ | $A_{1t}$ 788 | $(A_1+E_1)_t$ 792 | $E_{1t}$ (797) |

In their residual-ray reflectivity measurements, Spitzer *et al.*[8] found phonon energies of $E_{1t}=794$ cm$^{-1}$ and $A_{1t}=786$ cm$^{-1}$, in good agreement with our values.

### B. Weak Modes

No angular variation of energy was observed for any weak mode. We are therefore only concerned with distinguishing between modes of the same symmetry by assigning values of $x=q/q_{max}$.

Weak $A_1$ and $E_1$ modes are possible only at $x=0.67$ in 6$H$ SiC. The $A_1$ modes were observed in infrared measurements (see Fig. 1) but the doublet structure at 504 and 508 cm$^{-1}$ was not previously resolved. The placement of the $E_1$ doublets on the planar branches is obvious. The $E_2$ modes can be placed either at $x=0.33$ or at $x=1$, with doublets at $x=0.33$ and singlets at $x=1$. Thus, the assignment of the low-energy $E_2$ modes to the planar acoustic branch is clear. However, only two $E_2$ lines, at 766 and 788 cm$^{-1}$, are available for the planar optic branch. The separation seems too large for a doublet, so we assign one line to each of the $x$ positions, in such a way as to give the planar optic branch a smooth slope. It is only for this assignment that we need to use a plausibility argument.

The energies of all lines assigned to $x\neq 0$ are shown in Table IV and in Fig. 8. The strong-mode results for $\theta=0°$ have also been included at $x=0$ in Fig. 8 to complete the "dispersion" curves. The separation of the doublets has been exaggerated in order to show them clearly in this drawing.

TABLE IV. Energies (in cm$^{-1}$) of weak phonon modes, with their representations and assignments to values of $x=q/q_{max}$ in the large zone. They are listed in the order in which they are plotted in Fig. 8. $B_1$ modes are forbidden (F.), and two expected components of doublets have not been observed (N.O.).

| Branch | $x=0.33$ | $x=0.67$ | $x=1$ |
|---|---|---|---|
| Axial optic | $B_1$ F.<br>$B_1$ F. | $A_1$ 889<br>$A_1$ N.O. | $B_1$ F. |
| Planar optic | $E_2$ 788<br>$E_2$ N.O. | $E_1$ 777<br>$E_1$ 769 | $E_2$ 766 |
| Axial acoustic | $B_1$ F.<br>$B_1$ F. | $A_1$ 508<br>$A_1$ 504 | $B_1$ F. |
| Planar acoustic | $E_2$ 149<br>$E_2$ 145 | $E_1$ 241<br>$E_1$ 236 | $E_2$ 262 |

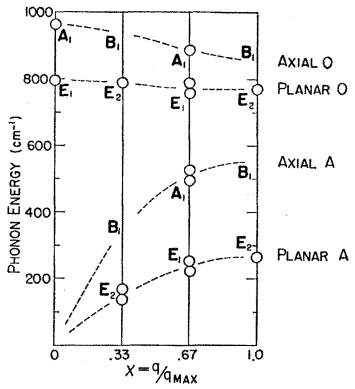


FIG. 8. Plot of experimental data in the form of dispersion curves in the large zone. The doublet separation is exaggerated. The energies of the strong modes ($x=0$) are listed in Table III, those of weak modes ($x\neq 0$) in Table IV. This figure is valid for weak modes with any phonon propagation direction, but is appropriate for the strong modes only when $\theta=0°$.

### C. Doublet Structure

The experimental data show four weak doublets with splittings ranging from 4 to 8 $cm^{-1}$. In each case the two components have the same symmetry, one doublet being $A_1$, one $E_2$, and two $E_1$. Because $A_1$ is a nondegenerate mode, and because $E_2$ is infrared *inactive*, their appearance in pairs is naturally attributed to the energy discontinuities within the large zone. For infrared-*active* $E_1$ modes, however, there is also the possibility of a longitudinal transverse (LT) splitting to lift the $E_1$ degeneracy, i.e., there are potentially quartets of lines at $x=0.67$, and there is no infrared data on these lines which would permit us to rule out LT splitting on the basis of infrared strength. We therefore used the fact that the LT splitting depends in a known way[20] on the phonon propagation angle $\theta$. We examined the 236, 241 $cm^{-1}$ doublet carefully at both $\theta=90°$ and 45°, and saw no change in the line positions. We conclude that these $E_1$ modes also have little infrared strength, the splitting being entirely due to the large-zone energy discontinuity. The other $E_1$ doublet, at 769 and 777 $cm^{-1}$, is very weak in the Raman spectrum and is obscured at $\theta=90°$.

If we assume that the LT splitting is not observable for any weak mode, the number of allowed weak Raman lines is 14, of which we have recorded 12 in Table IV. The two not observed (N.O. in Table IV) are components of doublets, and we have found experimentally that most of the doublets have one very weak component. All observed narrow lines have a logical place on the dispersion curves.[21] Broader lines observed as background in Fig. 3(a) are probably part of the two-phonon spectrum, which is strongest in $A_1$ symmetry combinations.

[20] Reference 11, p. 432.

## V. SUMMARY

The experimental observation of strong and weak groups of first-order Raman lines is correlated with the unusual polytype structure of 6*H* SiC through the use of a large zone. In general, the large-zone concept is useful when energy discontinuities within the zone are small; this is the case for 6*H* SiC, and the doublets in the Raman spectrum give the first accurate measurements of the 4–8-$cm^{-1}$ discontinuities.

Also related to the polytype structure is the fact that some of the weak modes are infrared active, yet have negligible infrared strength. They are extreme examples of normal modes in which the effect of crystal anisotropy is large compared with the effect of the long-range Coulomb field.

The use of laser excitation enabled us to observe all strong modes and 12 of the possible 14 weak modes. The normal-mode symmetries were identified by the use of polarized light, and the results were plotted in the form of dispersion curves. The concept of a common phonon spectrum for all SiC polytypes[10] suggests that Raman measurements on other polytypes may be used to fill out the dispersion curves. It is encouraging that energy discontinuities within the large zone are small. Raman scattering experiments are now being done on two other SiC polytypes.

The phonons reported here differ greatly in energy from those observed in luminescence[4] because the latter have $q$ vectors determined by the positions of the conduction-band minima; contrary to some speculation,[9] the conduction-band minima of 6*H* SiC are *not* on the symmetry axis.

[21] The search for weak narrow lines was more thorough in regions where they were expected, but the full spectral range was examined carefully enough to find any but extremely weak lines